

# Ready, Set, Grow – From Micelles to Giant Vesicles via Biocatalytic Activation

*Nicholas P. Bair,<sup>1</sup> Qinyu Zhu,<sup>2</sup> Byron A. Staynings,<sup>1</sup> Douglas R. Tree\*<sup>2</sup>, Walter F. Paxton\*<sup>1</sup>*

---

<sup>1</sup> Department of Chemistry and Biochemistry, Brigham Young University, Provo, UT 84602, USA

<sup>2</sup> Department of Chemical Engineering, Brigham Young University, Provo, UT 84602, USA

\*Corresponding authors

Walter F. Paxton  
Department of Chemistry and Biochemistry  
Brigham Young University  
C100 BNSN  
Provo, UT 84602  
Tel: +1 (801) 422 4917  
E-Mail: [paxton@chem.byu.edu](mailto:paxton@chem.byu.edu)

Douglas R. Tree  
Department of Chemical Engineering  
Brigham Young University  
330 EB  
Provo, UT 84602  
Tel: +1 (801) 422 5162  
E-Mail: [tree.doug@byu.edu](mailto:tree.doug@byu.edu)

**KEYWORDS.** self-assembly • surfactant • pH responsive • coarse-grained • morphology • micelles • vesicles • biocatalysis

## **ABSTRACT**

Controlling physicochemical processes that drive changes in supramolecular aggregates is an important objective toward creating artificial soft micro- and nanomachines. Previous research explored morphology control of membrane-based materials subjected to externally imposed chemical stimuli. Here we modulate the microscale morphology of pH-responsive assemblies by using biocatalysis to internally generate changes in global pH. Catalytic reactions offer flexibility in the mechanism and rate that stimuli are introduced to responsive assemblies, ultimately enabling precision and control over size and morphology. We observed, by dynamic light scattering and fluorescence microscopy, substantial microscale differences between assemblies subjected to manually titrated pH changes compared to biocatalytically-activated pH changes, including the growth of giant vesicles from micelles. Coarse-grained molecular dynamics simulations of these metastable self-assembled structures provided insight into the thermodynamics and kinetics of preferred structures. These results demonstrate the feasibility of using biocatalytic reactions to modulate the size and morphology of supramolecular assemblies from micelles to giant vesicles.

## INTRODUCTION

One longstanding goal in nanotechnology is to create life-like synthetic cells that exhibit autonomous behavior in response to environmental cues and programmed instructions. Mastering physicochemical principles that govern organization and reconfiguration of supramolecular assemblies, including bilayer membranes, would provide insights into biological processes that regulate changes in membrane morphology and properties and offer exciting opportunities to exploit these processes in artificial soft nanomachines with life-like properties and functions.

Chemical methods offer attractive approaches to drive and modulate the assembly of supramolecular systems.<sup>1-9</sup> Assembly of micelles and vesicles are of particular interest because they allow straightforward and unambiguous monitoring of morphological transformations.<sup>10-12</sup> These transitions can be activated by chemical modification (e.g. hydrolysis,<sup>13</sup> proteolysis<sup>12</sup> or covalent coupling<sup>14, 15</sup>), and by proton transfer to change the charge of surfactant headgroups.<sup>10, 16</sup> Stimuli activating these chemical processes are typically introduced from an external source (e.g. by solution addition) and mixed to provide homogenous distribution throughout the solution.

Catalytic and biocatalytic reactions in particular have great potential for modulating the shape and properties of supramolecular assemblies<sup>17-19</sup> and membranes.<sup>9, 12, 20-22</sup> Exploiting catalytic and biocatalytic reactions to stimulate responsive assemblies and membranes has several advantages over externally-imposed chemical stimuli, including: i) translating chemical signals that do not stimulate responsive assemblies – e.g. the substrate on which the catalyst acts – into chemical signals that do – e.g. a change in solution pH; ii) less disruptive and uniform introduction of chemical stimuli without mixing; and iii) the ability to exploit a range of aqueous-phase catalysts and enzymes to activate responsive assemblies.

We hypothesized that in addition to predictable changes in morphology driven to equilibrium states in response to specific stimuli, catalytic and biocatalytic activation may enable different mechanisms and rates of supramolecular assembly that could have a profound effect on preferred morphology and offer versatile ways to control it. Specifically, we hypothesized that introducing stimuli via biocatalytic reactions compared to manual titration would result in different sizes or microscale morphologies of supramolecular aggregates. In this way, biocatalysis could expand the versatility of stimuli-responsive assemblies ultimately enabling precision and control over size and morphology.

To demonstrate this, we compared the microscale aggregation behavior of the pH-responsive surfactant, (S)-O-methyl-serine dodecylamide hydrochloride (MSDH, Figure 1), to pH changes that are either externally imposed via manual titration or internally generated via biocatalysis. MSDH is a known lysosomotropic agent that has demonstrated<sup>23</sup> unique interactions with cellular membranes and the lysosome, depending on the pH-responsive morphology of its aggregates. This property has important implications for cell toxicity and drug delivery, and makes it an excellent candidate for testing biocatalytically activated morphology transformations. MSDH has previously demonstrated pH-responsive supramolecular transformations from micelles-to-vesicles as the pH was titrated from 3-12,<sup>11</sup> a consequence of the change in headgroup size and packing parameter. In comparison to manual titration, we used the biocatalyst *urease* to translate urea into a pH increase<sup>24, 25</sup> that drives the micelle-to-vesicle transition. We monitored microscale changes in aggregation behavior using dynamic light scattering and fluorescence microscopy. We compared these *in vitro* results to course-grained molecular dynamics simulations, which predicted phase behavior and kinetics of MSDH aggregates as a function of pH. These results confirmed the

feasibility of using biocatalytic reactions to modulate aggregate size and morphology that could be exploited to actuate artificial soft machines.

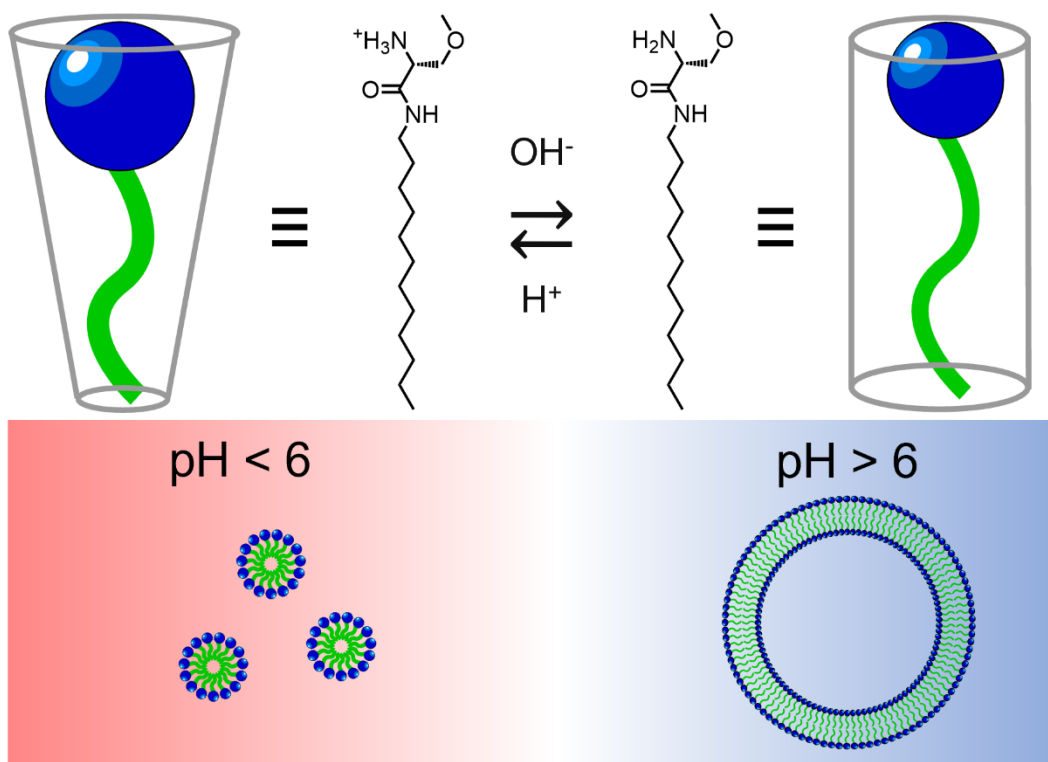


**Figure 1.** Structure and schematic of pH-responsive (S)-O-methyl-serine dodecylamide hydrochloride (MSDH), which produces smaller aggregates attributed to micelles below pH 6 and vesicular aggregates above pH 6.

## MATERIALS AND METHODS

**MSDH Sample Preparation.** (S)-O-methyl-serine dodecylamide hydrochloride (MSDH, Avanti Polar Lipids, 850546); Texas Red 1,2-dihexadecanoyl-sn-glycero-3-phosphoethanolamine, triethylammonium salt (TR-DHPE, Thermo Fisher T1395MP); urea (Sigma Aldrich, U1250); and 1U/mg Jack Bean Urease (Sigma Aldrich, 94280) were all purchased from commercial suppliers

and used without further purification. Deionized water was prepared from a commercial water purification system (Synergy V-R Millipore). MSDH stock solution, including 1 mol% of TR-DHPE, was dissolved in chloroform ( $\text{CHCl}_3$ ) and used to create the MSDH films for each experiment. MSDH films were rehydrated in aqueous solutions of 150 mM NaCl and 50 mM urea for manual titration and urease experiments to a concentration of 0.5 mg/mL MSDH and 1 mol% TR-DHPE. The rehydrated samples were sonicated in an E/MC RAI ultrasonic cleaner for 5 min and placed at room temperature for 1 h. They were then filtered 13 times through 0.1  $\mu\text{m}$  pore size polycarbonate membrane filters (Nuclepore). The pH of these suspensions was measured as a starting point for pH change experiments.

**Dynamic Light Scattering.** We used dynamic light scattering (DLS) to monitor the changes in aggregate size and the polydispersities of our samples. Scattered light intensities and correlation functions were collected using a Malvern Instruments Zetasizer Nano ZS instrument equipped with a 4 mW 633-nm laser, at a scattering detection angle of  $173^\circ$ . The cumulants analysis of correlograms measured by DLS was used semi-quantitatively to compare the apparent average sizes and the polydispersity indices (PDI) of MSDH aggregates in our experiments. However, the quantitative use of z-average from the cumulants analysis of DLS measurements in these experiments was tempered by two important factors: 1) confocal microscopy indicated that the size distributions of suspensions as the pH was changed were very broad (PDI=1) and 2) the size of the objects observed by microscopy was outside the useful quantitative range of DLS ( $<6 \mu\text{m}$ ).<sup>26</sup> The cumulants analysis algorithm was not modified from default settings, and as a result the fits were not always ideal. To prevent the overinterpretation of the size and PDI provided by the cumulants analysis, we consider the data semi-quantitatively for relative comparisons and refer to the measured z-average as the “apparent z-average”.

**Manual Titration.** For manual titrations suspensions were analyzed after the pH stabilized for each step. At least three measurements were performed at each pH. For manual titration experiments, MSDH solutions as described above were prepared. From the starting pH, small amounts of filtered 0.3 mM NaOH with the same osmolarity of the MSDH rehydration solution within 5 % of 295 Osm/L. NaOH solutions were filtered using a 0.2  $\mu\text{m}$  polyethersulfone membrane pore sized membrane filter (VWR 76479-024). The pH was raised from near 5.2 to 7.0 in small increments ( $\sim 0.15$ - $0.25$  pH units at a time). We measured the apparent z-average size of the MSDH aggregates after each addition of NaOH by DLS.

**Biocatalytic Activation.** For biocatalytic activation experiments, MSDH solutions as described above were prepared. Urease was added to a concentration of 0.0073 mg/mL such that the pH change by urease/urea was in the same range as the manual titration. These solutions were split into two fractions: one fraction was used for DLS measurements, and the other fraction was used for simultaneous pH measurements, both of which were monitored continuously as the reaction proceeded.

**Fluorescence Microscopy.** Samples for fluorescence microscopy (FM) and laser-scanning confocal microscopy (LSCM) characterization were placed on a glass slide with a SecureSeal<sup>TM</sup> image spacer from Millipore Sigma and a Corning 1-1/2 25  $\times$  25 mm cover slip. Fluorescence microscopy images were acquired with a Nikon Eclipse Ti2 microscope using a 40 $\times$  air objective. LSCM images in the main text were acquired using a LEICA TCS SP8 confocal microscope fitted with a HC PL APO 63 $\times$ /1.40 Oil CS2 objective and a HyD detection system (Leica Microsystems).

**Rheology Viscosity Measurements.** Samples for viscosity measurements were prepared for manual titration as mentioned above. The solution viscosity was measured at three different pH values corresponding to the three size regimes observed in DLS measurements. Manual titration

was performed to ensure no changes in pH would occur during analysis. Measurements were performed using an Anton Paar MRC 302 rheometer using a PP-25 measuring device. The temperature was set to 20 °C. the shear rate was set at  $10 \text{ s}^{-1}$  and was held constant for the measurements. 30 points were taken for each sample.

## RESULTS AND DISCUSSION

**Morphology Manipulation via Manual Titration.** We first confirmed the previously-demonstrated<sup>11</sup> pH-responsive aggregation behavior in manually-titrated MSDH solutions. Aqueous MSDH solutions – including 0.5 mg/mL MSDH, <5 µg/mL fluorescent lipid TR-DHPE, 150 mM NaCl, and 50 mM urea – were subjected to variable pH conditions controlled by manual titration with NaOH. We identified three distinct pH regimes that affected MSDH aggregation behavior: pH<6, pH=6, and pH>6. At pH<6, MSDH formed small aggregates, with apparent z-average diameters <100 nm, inferred from dynamic light scattering (DLS) measurements (Figure 2). The diameters of these aggregates were larger than the expected ~4-5 nm for spherical MSDH micelles and indicated the possibility of larger aggregates with different morphologies. Fluorescence microscopy images (Figure S1a) of MSDH suspensions at pH<6 revealed a uniform fluorescent background due to TR-DHPE label incorporated into MSDH aggregates at this pH, but discrete fluorescent aggregates were not observed. This result was consistent with micelles or aggregates <100 nm that cannot be easily resolved by fluorescence microscopy.

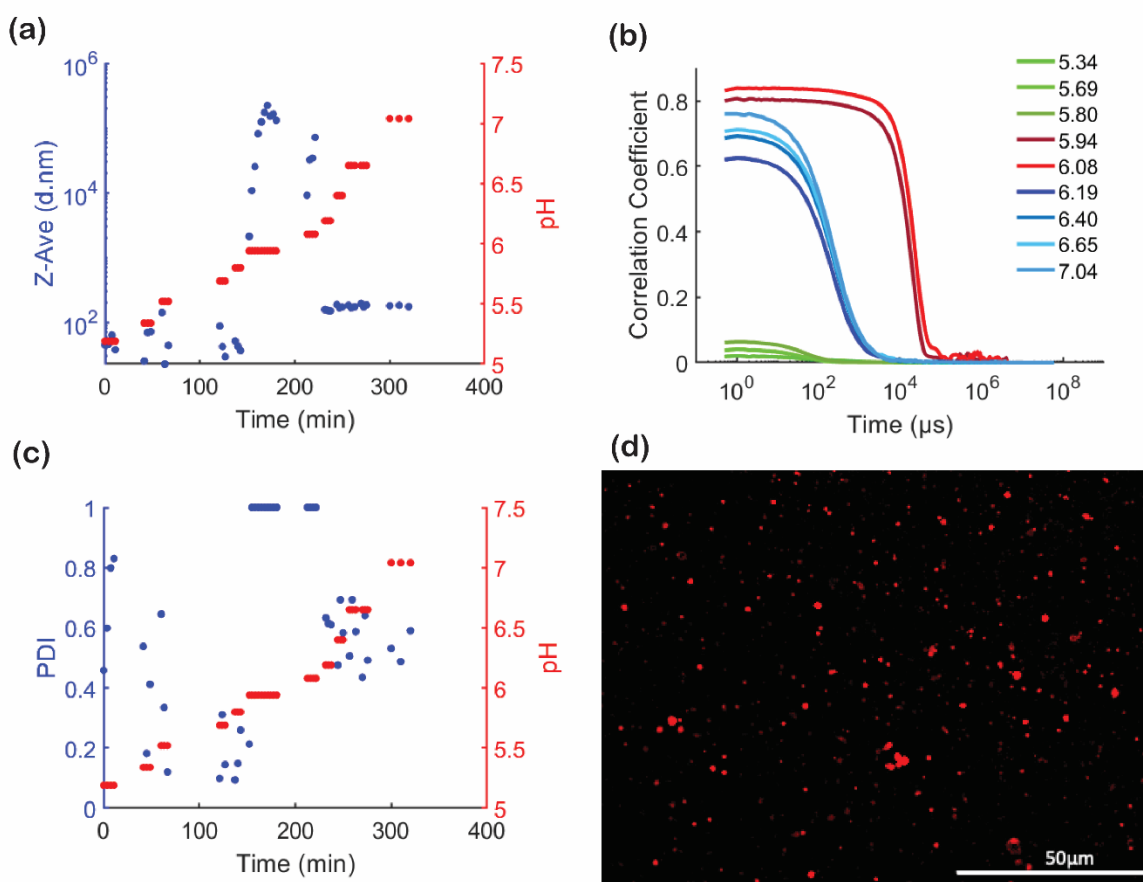


**Figure 2.** pH-responsive behavior of manually titrated aqueous MSDH suspensions (0.5 mg/mL MSDH;  $<5 \mu\text{g/mL}$  fluorescent lipid TR-DHPE; 50 mM urea; 150 mM NaCl). (a) Aggregate apparent z-average (note the logarithmic scale) obtained from cumulants analysis of correlograms obtained from DLS analysis of MSDH aggregates responding to manually titrated pH changes as a function of time. (b) Correlograms of the regions  $\text{pH}<6$   $\text{pH}=6$ , and  $\text{pH}>6$  legend contains the pH values. (c) Polydispersity index (PDI) of manual titration as a function of time and pH from cumulants analysis of correlograms from DLS measurements. (d) LSCM image of manually titrated MSDH suspensions at  $\text{pH}=7$ .

When these MSDH solutions were manually titrated with NaOH, DLS data suggested these aggregates grew to 100-200 nm at pH>6 (Figure 2a). Laser scanning confocal microscopy (LSCM) of these samples revealed microscale aggregation into structures as large as 1-5  $\mu\text{m}$ , but none that could be unambiguously identified by DLS or LSCM as vesicles (Figure 2d). Although microscale aggregates were visible at pH>6, the default cumulants analysis fits of the correlograms from DLS indicated a large fraction of smaller 100-200 nm aggregates. Nevertheless, both results were qualitatively consistent that the solution contained small (faster diffusing) MSDH aggregates under acidic conditions and larger (slower diffusing) aggregates at more neutral/basic pH.

Smaller aggregates at pH<6 and larger aggregates at pH>6 were previously attributed to micelles and vesicles, respectively.<sup>11</sup> This change in apparent size is evident in the correlograms where the lag time changes before the correlation decays (Figure 2b). It is important to note that at pH<6 the correlograms were noisy and their y-intercepts were very low (Figure 2b). This was due to very little light scattering from the sample at low pH. We also reported the polydispersity index (PDI) and pH vs time to show there is a broad distribution of sizes reported by the DLS (Figure 2c). Because the PDI from the cumulants analysis was so large (PDI=1), we could not use z-average diameter as a quantitative hydrodynamic diameter. Instead, we used changes in measured z-average diameter semi-quantitatively to indicate relative shifts in the average “apparent z-average diameter.”

Curiously, at pH=6, the approximate pK<sub>a</sub> of MSDH, DLS analysis indicated structures with apparent diameters >6  $\mu\text{m}$ , significantly larger than micelles or 100-200 nm diameter vesicles previously reported,<sup>11</sup> and beyond the upper limit of the measurable size range. These large-scale MSDH aggregates at pH=6, which have not to our knowledge been previously observed, were an interesting and perplexing surprise. In addition to the DLS data, we visually observed oil-like

droplets separating out when the sample was left undisturbed for 2 h (Figure S3). Based on the observed macroscale separation into discrete phases at pH=6, we hypothesized that this was a liquid-liquid phase separation (LLPS) of an MSDH-rich oily phase from an MSDH-poor aqueous phase. Above the  $pK_a$ , this phase separation faded as the droplets dispersed into smaller structures.

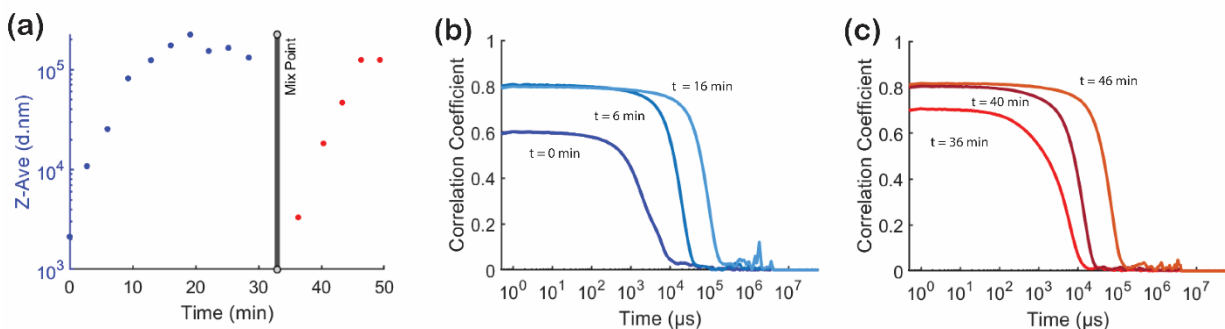


**Figure 3** DLS measurements before and after agitation at pH 6. (a) The apparent z-average size of the aggregates before and after agitation. DLS data is shown 30 min before mixing, after which the solution was removed from the instrument and mixed by pipetting the solution up and down approximately 10 times. The suspension was then placed in the DLS instrument and the apparent z-average size is reported for an additional 20 minutes. Correlograms for before (blue) and after (red) agitation are represented in panels (b) and (c).

To further investigate this hypothesis, we observed that minor disturbances, such as picking up the sample, broke up droplets of the oil-like phase. If these droplets are truly the product of a bulk LLPS, then they should proceed to coarsen into larger and larger droplets following mixing. To test this, we mixed the solution at pH 6 and compared DLS measurements before and after agitation (Figure 3). Upon mixing, the apparent z-average diameter decreased sharply followed by

a gradual increase, consistent with shear-induced breakup followed by coarsening of an MSDH-rich phase. The correlograms before agitation showed that the droplets increased in size with time, consistent with coarsening, and the trend repeated itself in the correlogram after agitation (Figure 3c). These results demonstrated that mixing greatly influenced the assembly/disassembly of MSDH.

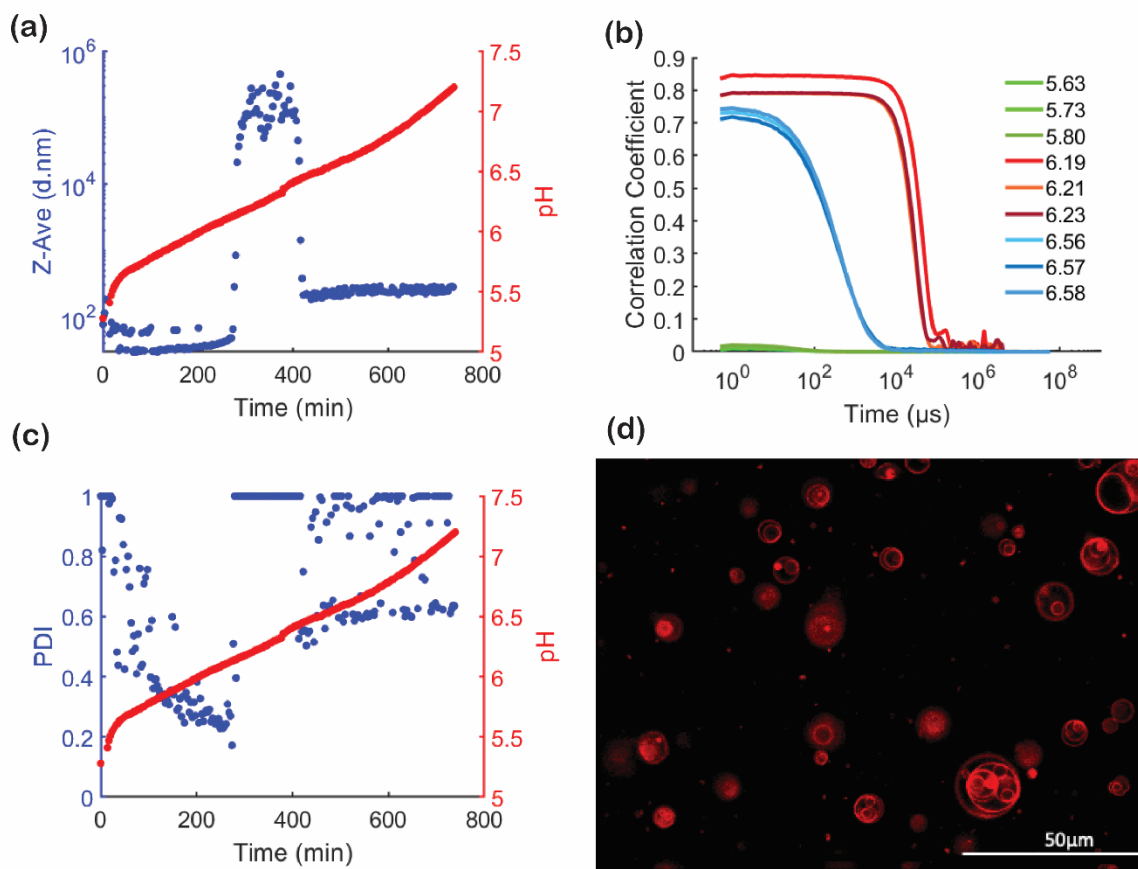


**Figure 4.** pH-responsive behavior of aqueous MSDH suspensions (0.5 mg/mL MSDH;  $<5\ \mu\text{g/mL}$  fluorescent lipid TR-DHPE; 50 mM urea; 150 mM NaCl). Aggregate apparent z-average (note the logarithmic scale), obtained from dynamic light scattering (DLS) measurements (see Supporting Information for details) of MSDH aggregates responding to biocatalytically-titrated

pH changes as a function of time (a). Correlograms of the regions pH<6, pH=6, and pH>6 legend contains the pH values (b). Polydispersity index (PDI) of manual titration as a function of time and pH (c). LSCM images of MSDH suspensions at pH=7 for manually titrated (d).

We sought to rule out gelation or some other change in solution viscosity as the source of the jump in apparent z-average size in the DLS data near pH 6. The z-average reported by DLS is inferred from the diffusivity  $D$  through the Stokes-Einstein equation,  $D = \frac{kT}{3\pi\eta d_H}$ , where  $d_H$  is the hydrodynamic diameter (approximated by the z-average diameter) and  $\eta$  is the solution viscosity. Thus, a change in the reported z-average size by DLS could be confused for a change in solution viscosity if gelation occurs.<sup>27</sup> We performed measurements of the viscosity of the 0.5 mg/mL MSDH solution in the three different regimes: pH<6, pH=6, and pH>6 (Figure S2). The viscosity in all regimes was within 15% of the expected viscosity for 150 mM aqueous NaCl (1.2 mPa·s) and showed no obvious trend. These differences in viscosity are clearly not large enough to account for the orders-of-magnitude change in the apparent z-average size in Figure 2a.

Based on the above observations and the coincidence of the critical pH of the LLPS to the  $pK_a$  of MSDH, we conclude that the solution undergoes a LLPS at pH=6 with the tentative hypothesis that the phase separation is a coacervation driven by hydrogen bonding. The number of hydrogen bond donors and acceptors are maximized at the  $pK_a$  of MSDH, where the fraction of protonated and deprotonated MSDH would be exactly equal. Additionally, there is precedence in the literature for pH-dependent coacervation in surfactant solutions<sup>28-30</sup> including coacervation driven by hydrogen bonding.<sup>31</sup> It is tempting to further speculate about the nature of this phase, its origin, additional properties (e.g., temperature and salt dependence), and applications. However, in order

to maintain focus on the present question of catalytically induced pH change on morphology, we leave further investigation for future work.

**Morphology Manipulation via Biocatalytic Activation.** Having characterized the behavior of MSDH aggregation by manual titration, we sought to influence MSDH aggregation behavior another way: biocatalytic activation. The decomposition of urea produces  $\text{CO}_2$  and  $\text{NH}_3$ , resulting in a net increase in pH. Using urease, we translated a chemical signal that does not affect MSDH aggregation (urea) into a chemical signal that does (pH), which we expected to affect MSDH aggregation behavior. Furthermore, because mixing can influence the size of MSDH droplets and supramolecular aggregates, we reasoned that changing pH using a method that does not require mixing could impact morphology.

We proceeded using suspensions of MSDH that were prepared in the same manner as those used for the manual titration with the addition of  $7.3 \mu\text{g/mL}$  of urease. Immediately following, the solution was gently agitated and was then left undisturbed for the remainder of the experiment to allow a uniform pH increase throughout the quiescent solution. Changes in pH were monitored simultaneously with DLS measurements. As with manual titration, the apparent z-average size of MSDH aggregates and the pH of the solutions are plotted versus time (Figure 4a). Corresponding correlograms are shown in Figure 4b. As reported for the manual titration protocol, the DLS measurements show three distinct regimes for  $\text{pH} < 6$ ,  $\text{pH} = 6$ , and  $\text{pH} > 6$ . A comparison of the DLS results between the biocatalytic activation protocol (Figure 2a and 2b) and the manual titration protocol (Figure 4a and 4b) shows similar trends in the correlogram shape and apparent z-average size as a function of pH. However, unlike in the manually titrated case, LSCM of biocatalytically activated MSDH aggregates revealed giant uni- and multilamellar vesicles for  $\text{pH} > 6$ , with some as large as  $20 \mu\text{m}$  in diameter (Figure 4d). The spontaneous growth of these vesicles was in stark

contrast to the smaller ill-defined aggregates observed with manual titration (Figure 2d). The PDI for the catalytically titrated system was large (close to one) and highly variable compared to the manually titrated case. This data provides additional evidence that the two protocols result in a substantially different morphology at  $\text{pH} > 6$ .

**Course-Grained Molecular Dynamics Simulations.** To provide additional insights into phase behavior and kinetics of aggregate reconfiguration, we performed coarse-grained molecular dynamics (CGMD) simulations in GROMACS.<sup>32</sup> Our computational model of the system included water, salt, MSDH (protonated and not), and co-ions modeled using the MARTINI 3 force field.<sup>33</sup> We simulated changes in pH by altering the fraction of MSDH in the simulation that was protonated. To overcome slow micellar equilibration, we used a solvent switching protocol<sup>34</sup> to obtain equilibrium structures. Details related to the coarse-grained model and the simulation protocol are given in the SI.

Due to computational constraints on simulation domain sizes ( $L \in [18,38]$  nm), our simulations required higher concentrations of MSDH (0.01 to 0.09 g/mL) and salt (0.84 M NaCl) than the experimental system (0.5 mg/mL MSDH with 0.15 M NaCl). The simulated concentrations were comparable to previous published CGMD studies using explicit solvent models.<sup>35, 36</sup> Despite these differences, the simulations were in the same qualitative regime as the experimental system: both were above the critical micelle concentration (CMC) ( $\sim 40 \mu\text{M}$  or 0.013 mg/mL),<sup>11</sup> and below the order-disorder transition for MSDH microphases. According to well-established theory, the micelle aggregation number is independent of concentration in this regime.<sup>37, 38</sup> Both systems showed disordered micellar aggregates with average intermicellar distances of  $D_M \approx 13$  nm in simulations with  $C_{\text{MSDH}} = 0.03$  g/mL and  $D_M \approx 2 \mu\text{m}$  for experiments (the latter estimated from the MSDH concentration and the average aggregate size).

The difference in salt concentration primarily impacted the Debye length,  $\lambda_D$ , and we expected that when  $\lambda_D \ll D_M$ , MSDH aggregates will not experience significant overlap of double layers. The Debye length in CGMD simulation was determined to be 0.33 nm, giving the ratio of Debye length to intermicellar distance  $R_L = \lambda_D/D_M = 0.025$ . The Debye length in experiments was 0.8 nm, giving an even smaller  $R_L = 4 \times 10^{-4}$ . Thus, while the concentrations of MSDH and salt were not numerically matched between simulations and experiments, we expected the simulated behavior to be qualitatively similar.

We first compared the results from the CGMD simulations to the experiments above in relation to our hypotheses concerning the morphology of MSDH as a function of pH. Figure 5a summarizes the equilibrium morphology diagram of the MSDH/water/salt system. At all concentrations, we observed a transition from spherical micelles at low pH to disk-like aggregates at intermediate pH to vesicles at high pH, interspersed with regions of mixed morphologies. The detailed pH values of these transitions are a function of MSDH concentration, but the transition from micelles to disk-like aggregates occurs around a pH of approximately 5.5 and the transition from disk-like aggregates to vesicles occurs in the range of pH values between 5.7 and 7.0. The morphology and the pH values of these transitions qualitatively agree with the experimental observations for  $\text{pH} < 6$  and  $\text{pH} > 6$ . However, there was no evidence in the simulation for a LLPS at  $\text{pH} = 6$ . Instead, the CGMD results predict that the morphology transitions from micelles to bilayers around the  $\text{pK}_a$  of MSDH with a curvature that smoothly increases, closing the bilayers into vesicles as the pH increases.

In addition to morphology, we calculated the average size and diffusivity of simulated MSDH aggregates at  $C_{\text{MSDH}} = 0.03 \text{ g/mL}$  as a function of protonation/pH (Figure 5b). As indicated by the blue curve in Figure 5b, the aggregation size steadily increases from 4 nm at 100% protonation

to around 7.5 nm at 60% protonation where it remains steady until 0% protonation. The change in slope corresponds to the transition from mixed micelles/bilayers to only bilayers. The corresponding diffusivity is shown by the red curve in Figure 5b. Diffusivity decreases from 100% protonation until 50% protonation, where it reaches a minimum and then recovers to a modestly larger value. We attributed the minimum to the combined effect of aggregate size and shape. Diffusivity mirrors aggregate size in the regimes where spherical micellar aggregates and vesicles are the dominant morphology. The minimum in the diffusivity corresponds to the region where the aggregates are flat bilayers. It is a well-known fact in colloidal hydrodynamics that the aspect ratio plays a significant role in diffusivity<sup>39, 40</sup> and clearly the anisotropic shape of the disks result in slower diffusion than spherical vesicles for a given aggregate size.

The morphology diagram and size/diffusivity calculations from the CGMD simulations provide a useful benchmark for comparing to the experimental data and for testing hypotheses, but there are some noteworthy limitations. For  $\text{pH} < 6$ , there is good qualitative agreement between the model and the experiments, and the model predicts a reasonable micelle size and diffusivity, though the DLS experiments are not sufficiently precise to make a quantitative comparison. For  $\text{pH} > 6$ , the simulation prediction of bilayers and vesicles is qualitatively consistent with experiments as well. The sizes of these aggregates are considerably smaller than those in experiments, but this is a well-known limitation of CGMD simulations because of the limited size of the computational domain. Additionally, bilayers and vesicles are metastable structures with little free energy difference between aggregates of different size,<sup>41, 42</sup> therefore the size of these structures is kinetically determined. Consequently, the difference in bilayer aggregate size between simulation and experiment is not a good test of the simulation accuracy.

The region of least agreement between the model and the experiment is at pH=6. Here the model predicts low-curvature bilayers, which likely corresponds to giant vesicles or flat bilayers (if it was possible to create extremely large computational domains). However, the model entirely misses the LLPS. While this qualitative disagreement with experiment is an important weakness, the model does not predict gelation or the formation of wormlike micelles, which are competing hypotheses to explain the DLS data that were ruled out by our viscosity measurements. We hypothesize that our CG mapping for MSDH or the parameterization of the MARTINI 3 force field lacks sufficient accuracy with regard to hydrogen bonding to capture the LLPS. It is also possible that the difference in the MSDH concentration, salt concentration, or the equilibration protocol (which involves the use of high temperatures) is responsible for the lack of agreement with experiment.

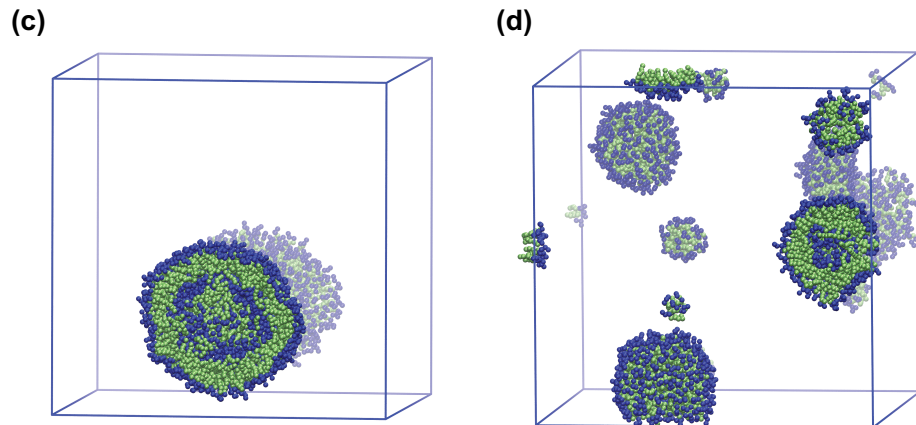
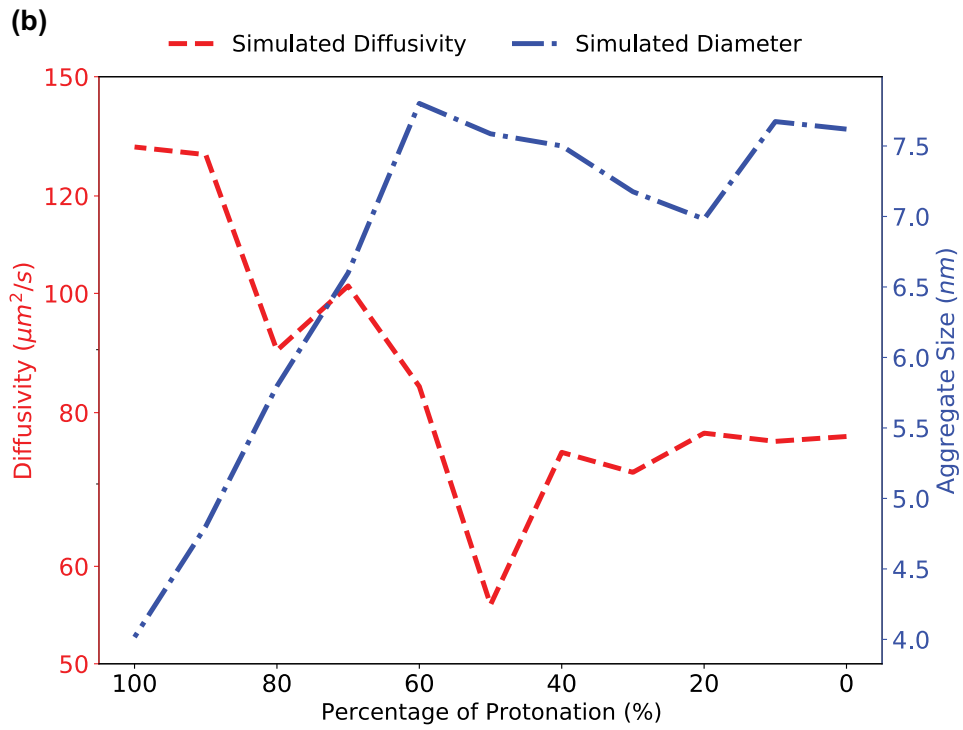
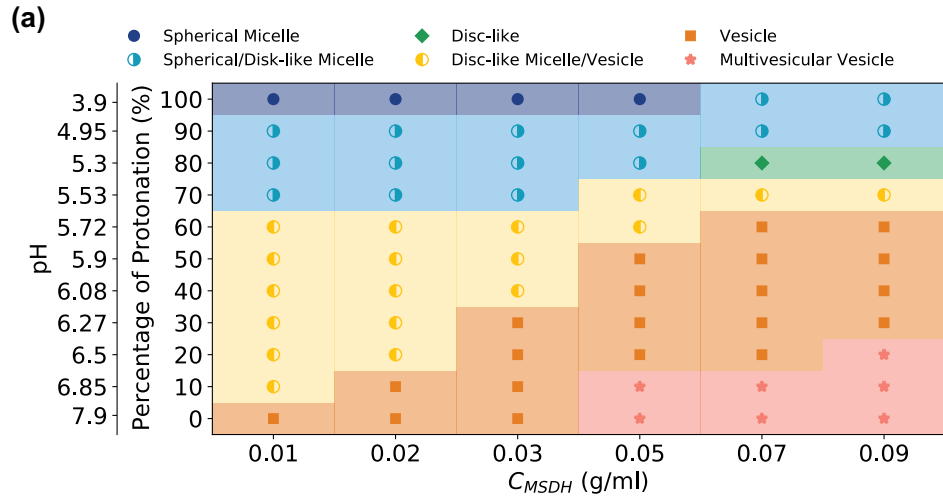


**Figure 5.** Simulation results of the MSDH/water/salt pH responsive system. (a) An equilibrium morphology diagram of MSDH aggregates as a function of concentration and percent protonation. Note that the x-axis is not numerically scaled, and pH decreases nonlinearly with increasing percent protonation of MSDH. (b) Simulated diffusivity and aggregation size as a function of percent protonation of MSDH at  $C_{\text{MSDH}}=0.03$  g/ml. A multivesicular assembly at  $C_{\text{MSDH}}=0.05$  g/ml and all deprotonated states (c) before shear, and (d) after shear. Blue particles represent the hydrophilic head group and green beads represent hydrophobic tails. Water molecules are omitted for better visualization.

Beyond morphology, the CGMD simulations provide additional insight into the different end-states of the manually titrated and internally generated systems as seen in the LSCM images in Figure 2c and 4c. We hypothesized that the manually titrated samples experience shear during pipetting that breaks up the large bilayer assemblies, whereas the biocatalytically driven pH change had no such disruption, enabling the growth of giant multilamellar vesicles. To investigate the effects of pipetting during manual titration, we simulated shear of multivesicular MSDH aggregates obtained from equilibrium simulations. We did so by first shearing the simulation box in each direction for 30 ns, and then removing the shear and allowing the system to relax for an additional 30 ns. Figure 5c and 5d show simulation snapshots before and after the shearing process. Aggregates that re-form after shear consisted of unilamellar vesicles and several smaller micelles. This morphology was consistent with the LSCM observations in Figure 2c. Average aggregate sizes also decrease with shear (from 10.40 nm to 4.58 nm, see SI for details), in qualitative agreement with the LSCM observations.

As was the case with the equilibrium simulations, it is important to emphasize that these simulations show the plausibility of the hypothesized mechanism but are not quantitative. Owing

to the small size of the simulation domain and the vesicle, the shear rate used in our non-equilibrium CGMD simulations was  $6.8 \times 10^{10} \text{ s}^{-1}$ , which is orders of magnitude larger than the experimental shear rate. Based on the pipetting rates and volumes used in our experiments, we estimated the shear experienced by MSDH aggregates in our samples to be on the order of  $400 \text{ s}^{-1}$ . To the best of our knowledge, the energetic penalties of dividing vesicle membranes comprised of single-tailed amphiphiles, like MSDH, have not been measured. However, vesicles comprised of single-tailed amphiphiles (oleic acid instead of MSDH) reportedly divide into smaller vesicles at shear rates as low as  $15 \text{ s}^{-1}$ .<sup>43</sup> We therefore suspect that the energy for disrupting MSDH vesicles are significantly lower than the energy cost of dividing *lipid* vesicles, which are reportedly on the order of 250-500 kT.<sup>44</sup> Consequently, our simulation results demonstrate that shear can break up vesicles of MSDH and that the kinetics for small aggregates to reassemble and reach equilibrium through chain exchange are quite slow. This provides a possible explanation of how biocatalytically induced pH change can lead to larger structures that are otherwise inaccessible using manual pipetting.

## CONCLUSIONS.

Biocatalytic reactions can be used to activate morphological transformations in supramolecular assemblies by translating chemical signals that do not affect pH-responsive assemblies (i.e., urea) into pH changes that do. Using urea/urease reaction to increase solution pH, we produced uniform pH changes that resulted in the spontaneous growth of giant uni- and multilamellar MSDH vesicles. These vesicles were significantly larger than aggregates generated via manual titration, demonstrating the potential for control over size and morphology of supramolecular assemblies using biocatalytic reactions. Additionally, we used CGMD simulations to produce a morphology

diagram for MSDH that provided insight into our experimental observations. This model adds additional weight to our hypothesis that low curvature bilayer aggregates may be responsible for the deep minimum in diffusivity seen in DLS, and that shear due to pipetting may be responsible for breaking up these aggregates and preventing the formation of giant multilamellar vesicles. The latter demonstrates the feasibility of catalytic reactions as non-invasive stimuli that can be used to precisely control self-assembled morphology. We anticipate that a wide range of aqueous phase catalysts and enzymes can also be used to activate responsive membranes in response to different chemical signals. Taken together, these results demonstrate the feasibility of using biocatalytic reactions to control the size and morphology of supramolecular assemblies for artificial soft machines. As demonstrated by Giraldo et.al.<sup>23</sup> the structure of MSDH has an impact on the action it takes when interacting with cellular membranes, and it may be possible to activate the lysosomotropic effects of MSDH through in vivo biocatalytic methods. Furthermore, coupling complementary biocatalytic reactions together could enable reaction networks and chemical systems that can be used to generate and control life-like properties and functions of artificial membranes, supramolecular assemblies, and soft nanomachines.

## **ASSOCIATED CONTENT**

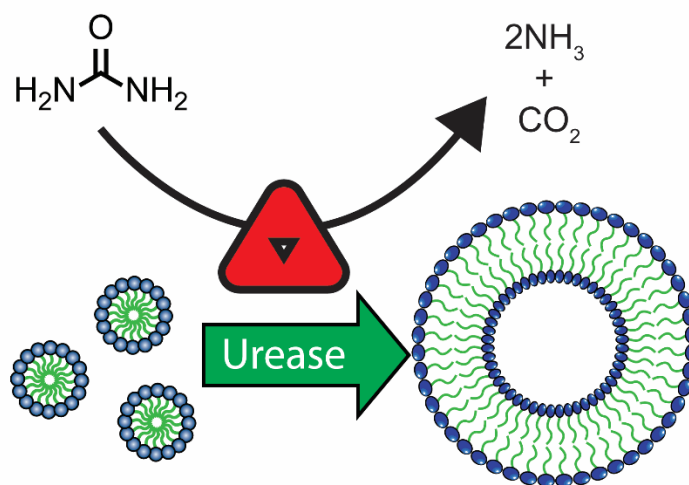
**Supporting Information.** Fluorescence micrographs and macroscale images of MSDH suspensions; Rheology measurements; Details of CGMS simulations (PDF); Cumulants and General Purpose fits to correlograms obtained by DLS.

**Author Contributions.** The manuscript was written through contributions of all authors.

**All authors have given approval to the final version of the manuscript.**

**Funding Sources.** This research was supported by a Brigham Young University Interdisciplinary Research Award from the Simmons Research Endowment (No. 101004366).

## TOC GRAPHIC



## REFERENCES

- (1) Boekhoven, J.; Hendriksen, W. E.; Koper, G. J. M.; Eelkema, R.; van Esch, J. H. Transient assembly of active materials fueled by a chemical reaction. *Science* **2015**, *349* (6252), 1075-1079. DOI: 10.1126/science.aac6103.
- (2) Trausel, F.; Maity, C.; Poolman, J. M.; Kouwenberg, D. S. J.; Versluis, F.; van Esch, J. H.; Eelkema, R. Chemical signal activation of an organocatalyst enables control over soft material formation. *Nature Communications* **2017**, *8* (1), 879. DOI: 10.1038/s41467-017-00998-3.
- (3) Wang, Y.; Versluis, F.; Oldenhof, S.; Lakshminarayanan, V.; Zhang, K.; Wang, Y.; Wang, J.; Eelkema, R.; Guo, X.; van Esch, J. H. Directed Nanoscale Self-Assembly of Low Molecular Weight Hydrogelators Using Catalytic Nanoparticles. *Adv. Mater.* **2018**, *30* (21), 1707408. DOI: doi:10.1002/adma.201707408.
- (4) Kodama, A.; Sakuma, Y.; Imai, M.; Oya, Y.; Kawakatsu, T.; Puff, N.; Angelova, M. I. Migration of phospholipid vesicles in response to  $\text{OH}^-$  stimuli. *Soft Matter* **2016**, *12* (11), 2877-2886, 10.1039/C5SM02220G. DOI: 10.1039/C5SM02220G.
- (5) Stachowiak, J. C.; Hayden, C. C.; Sasaki, D. Y.; Whitesides, G. M. Steric confinement of proteins on lipid membranes can drive curvature and tubulation. *Proceedings of the National Academy of Sciences of the United States of America* **2010**, *107* (17), 7781-7786. JSTOR.
- (6) Nawa, E.; Nishigaki, Y.; Yamamoto, D.; Shioi, A. Rhythmic shape change of a vesicle under a pH gradient. *Soft Matter* **2013**, *9* (32), 7832-7842, Article. DOI: 10.1039/c3sm51100f.

- (7) Christian, D. A.; Tian, A.; Ellenbroek, W. G.; Levental, I.; Rajagopal, K.; Janmey, P. A.; Liu, A. J.; Baumgart, T.; Discher, D. E. Spotted vesicles, striped micelles and Janus assemblies induced by ligand binding. *Nature materials* **2009**, *8* (10), 843-849. DOI: 10.1038/nmat2512 PubMed.
- (8) Shin, S. H. R.; McAninch, P. T.; Henderson, I. M.; Gomez, A.; Greene, A. C.; Carnes, E. C.; Paxton, W. F. Self-assembly/disassembly of giant double-hydrophilic polymersomes at biologically-relevant pH. *Chem. Commun.* **2018**, *54* (65), 9043-9046. DOI: 10.1039/c8cc05155k.
- (9) Holló, G.; Miele, Y.; Rossi, F.; Lagzi, I. Shape changes and budding of giant vesicles induced by an internal chemical trigger: an interplay between osmosis and pH change. *Physical Chemistry Chemical Physics* **2021**, *23* (7), 4262-4270, 10.1039/D0CP05952H. DOI: 10.1039/D0CP05952H.
- (10) Lagzi, I.; Wang, D. W.; Kowalczyk, B.; Grzybowski, B. A. Vesicle-to-Micelle Oscillations and Spatial Patterns. *Langmuir* **2010**, *26* (17), 13770-13772, Article. DOI: 10.1021/la102635w.
- (11) Giraldo, A. M. V.; Fyrner, T.; Wennmalm, S.; Parikh, A. N.; Ollinger, K.; Ederth, T. Spontaneous Vesiculation and pH-Induced Disassembly of a Lysosomotropic Detergent: Impacts on Lysosomotropism and Lysosomal Delivery. *Langmuir* **2016**, *32* (50), 13566-13575. DOI: 10.1021/acs.langmuir.6b03458.
- (12) Wright, D. B.; Ramírez-Hernández, A.; Touve, M. A.; Carlini, A. S.; Thompson, M. P.; Patterson, J. P.; de Pablo, J. J.; Gianneschi, N. C. Enzyme-Induced Kinetic Control of Peptide–Polymer Micelle Morphology. *ACS Macro Letters* **2019**, *8* (6), 676-681. DOI: 10.1021/acsmacrolett.8b00887.
- (13) Toyota, T.; Takakura, K.; Kose, J.; Sugawara, T. Hierarchical Dynamics in the Morphological Evolution from Micelles to Giant Vesicles Induced by Hydrolysis of an Amphiphile. *ChemPhysChem* **2006**, *7* (7), 1425-1427. DOI: <https://doi.org/10.1002/cphc.200600176>.
- (14) Hardy, M. D.; Yang, J.; Selimkhanov, J.; Cole, C. M.; Tsimring, L. S.; Devaraj, N. K. Self-reproducing catalyst drives repeated phospholipid synthesis and membrane growth. *Proceedings of the National Academy of Sciences* **2015**, *112* (27), 8187. DOI: 10.1073/pnas.1506704112.
- (15) Maiti, S.; Fortunati, I.; Ferrante, C.; Scrimin, P.; Prins, L. J. Dissipative self-assembly of vesicular nanoreactors. *Nature Chemistry* **2016**, *8* (7), 725-731, Article. DOI: 10.1038/nchem.2511.
- (16) Peterlin, P.; Arrigler, V.; Kogej, K.; Svetina, S.; Walde, P. Growth and shape transformations of giant phospholipid vesicles upon interaction with an aqueous oleic acid suspension. *Chem. Phys. Lipids* **2009**, *159* (2), 67-76, Article. DOI: 10.1016/j.chemphyslip.2009.03.005.
- (17) Heuser, T.; Weyandt, E.; Walther, A. Biocatalytic Feedback-Driven Temporal Programming of Self-Regulating Peptide Hydrogels. *Angewandte Chemie-International Edition* **2015**, *54* (45), 13258-13262. DOI: 10.1002/anie.201505013.
- (18) Martin, N.; Douliez, J.-P.; Qiao, Y.; Booth, R.; Li, M.; Mann, S. Antagonistic chemical coupling in self-reconfigurable host–guest protocells. *Nature Communications* **2018**, *9* (1), 3652. DOI: 10.1038/s41467-018-06087-3.

- (19) Del Giudice, D.; Fratello, F.; Sappino, C.; Di Stefano, S. Chemical Tools for the Temporal Control of Water Solution pH and Applications in Dissipative Systems. *Eur. J. Org. Chem.* **2022**, 2022 (33), e202200407. DOI: <https://doi.org/10.1002/ejoc.202200407>.
- (20) Zhu, Q.; Scott, T. R.; Tree, D. R. Using reactive dissipative particle dynamics to understand local shape manipulation of polymer vesicles. *Soft Matter* **2021**, 17 (1), 24-39. DOI: 10.1039/d0sm01654c.
- (21) Zhu, Q.; Tree, D. R. Simulations of Morphology Control of Self-Assembled Amphiphilic Surfactants. *Journal of Polymer Science* **2023**, in press. DOI: 10.1002/pol.20220771.
- (22) Miele, Y.; Medveczky, Z.; Holló, G.; Tegze, B.; Derényi, I.; Hórvölgyi, Z.; Altamura, E.; Lagzi, I.; Rossi, F. Self-division of giant vesicles driven by an internal enzymatic reaction. *Chem Sci* **2020**, 11 (12), 3228-3235. DOI: 10.1039/c9sc05195c From NLM.
- (23) Villamil Giraldo, A. M.; Eriksson, I.; Wennmalm, S.; Fyrner, T.; Ederth, T.; Öllinger, K. Interactions of the Lysosomotropic Detergent O-Methyl-Serine Dodecylamide Hydrochloride (MSDH) with Lipid Bilayer Membranes-Implications for Cell Toxicity. *Int J Mol Sci* **2020**, 21 (9). DOI: 10.3390/ijms21093136 From NLM.
- (24) Russell, A. J.; Erbeldinger, M.; DeFrank, J. J.; Kaar, J.; Drevon, G. Catalytic buffers enable positive-response inhibition-based sensing of nerve agents. *Biotechnol. Bioeng.* **2002**, 77 (3), 352-357. DOI: 10.1002/bit.10152 From NLM.
- (25) Hu, G.; Pojman, J. A.; Scott, S. K.; Wrobel, M. M.; Taylor, A. F. Base-Catalyzed Feedback in the Urea-Urease Reaction. *The Journal of Physical Chemistry B* **2010**, 114 (44), 14059-14063. DOI: 10.1021/jp106532d.
- (26) Malvern's General Purpose fitting algorithm overfit the data to multimodal distributions (3-4 discrete peaks that varied greatly in size and intensity in intensity distribution plots) in what was expected to be a monomodal distribution of aggregates with a very broad polydispersity index (PDI=1). For comparison, standard cumulants and General Purpose fits for representative samples can be found in the Supporting Information, Figures S7-S12.
- (27) Ruenraroengsak, P.; Florence, A. T. The diffusion of latex nanospheres and the effective (microscopic) viscosity of HPMC gels. *Int. J. Pharm.* **2005**, 298 (2), 361-366. DOI: <https://doi.org/10.1016/j.ijpharm.2005.01.044>.
- (28) Huang, X.; Cao, M.; Wang, J.; Wang, Y. Controllable Organization of a Carboxylic Acid Type Gemini Surfactant at Different pH Values by Adding Copper(II) Ions. *The Journal of Physical Chemistry B* **2006**, 110 (39), 19479-19486. DOI: 10.1021/jp0630121.
- (29) Zhao, W.; Wang, Y. Coacervation with surfactants: From single-chain surfactants to gemini surfactants. *Adv. Colloid Interface Sci.* **2017**, 239, 199-212. DOI: <https://doi.org/10.1016/j.cis.2016.04.005>.
- (30) Wang, M.; Wang, Y. Development of surfactant coacervation in aqueous solution. *Soft Matter* **2014**, 10 (40), 7909-7919, 10.1039/C4SM01386G. DOI: 10.1039/C4SM01386G.
- (31) Peng, L.; Feng, A.; Huo, M.; Yuan, J. Ferrocene-based supramolecular structures and their applications in electrochemical responsive systems. *Chem. Commun.* **2014**, 50 (86), 13005-13014, 10.1039/C4CC05192K. DOI: 10.1039/C4CC05192K.
- (32) Lindahl; Abraham; Hess; Spoel, v. d. *GROMACS 2021.4 Manual*; Zenodo, 2021. DOI: 10.5281/zenodo.5636522.
- (33) Souza, P. C. T.; Alessandri, R.; Barnoud, J.; Thallmair, S.; Faustino, I.; Grünwald, F.; Patmanidis, I.; Abdizadeh, H.; Bruininks, B. M. H.; Wassenaar, T. A.; et al. Martini 3: a general purpose force field for coarse-grained molecular dynamics. *Nat. Methods* **2021**, 18 (4), 382-388. DOI: 10.1038/s41592-021-01098-3.

- (34) Dong, M.; Wessels, M. G.; Lee, J. Y.; Su, L.; Wang, H.; Letteri, R. A.; Song, Y.; Lin, Y.-N.; Chen, Y.; Li, R.; et al. Experiments and Simulations of Complex Sugar-Based Coil-Brush Block Polymer Nanoassemblies in Aqueous Solution. *ACS Nano* **2019**, *13* (5), 5147-5162. DOI: 10.1021/acsnano.8b08811.
- (35) Kraft, J. F.; Vestergaard, M.; Schiøtt, B.; Thøgersen, L. Modeling the Self-Assembly and Stability of DHPC Micelles Using Atomic Resolution and Coarse Grained MD Simulations. *Journal of Chemical Theory and Computation* **2012**, *8* (5), 1556-1569. DOI: 10.1021/ct200921u.
- (36) de Souza, R. M.; Ratochinski, R. H.; Karttunen, M.; Dias, L. G. Self-Assembly of Phosphocholine Derivatives Using the ELBA Coarse-Grained Model: Micelles, Bicelles, and Reverse Micelles. *Journal of Chemical Information and Modeling* **2020**, *60* (2), 522-536. DOI: 10.1021/acs.jcim.9b00790.
- (37) Moroi, Y. *Micelles: Theoretical and Applied Aspects*; Springer Science+Business Media, 1992. DOI: 10.1007/978-1-4899-0700-4.
- (38) Israelachvili, J. N. *Intermolecular and Surface Forces*; Academic Press, 2011.
- (39) Ortega, A.; García de la Torre, J. Hydrodynamic properties of rodlike and disklike particles in dilute solution. *The Journal of Chemical Physics* **2003**, *119* (18), 9914-9919. DOI: 10.1063/1.1615967 (accessed 5/20/2024).
- (40) Wang, J.; Yang, Y.; Yu, M.; Hu, G.; Gan, Y.; Gao, H.; Shi, X. Diffusion of rod-like nanoparticles in non-adhesive and adhesive porous polymeric gels. *Journal of the Mechanics and Physics of Solids* **2018**, *112*, 431-457. DOI: <https://doi.org/10.1016/j.jmps.2017.12.014>.
- (41) Luisi, P. L. Are Micelles and Vesicles Chemical Equilibrium Systems? *J. Chem. Educ.* **2001**, *78* (3), 380. DOI: 10.1021/ed078p380.
- (42) Stano, P.; Luisi, P. L. Achievements and open questions in the self-reproduction of vesicles and synthetic minimal cells. *Chem. Commun.* **2010**, *46* (21), 3639-3653. DOI: 10.1039/b913997d.
- (43) Zhu, T. F.; Szostak, J. W. Coupled Growth and Division of Model Protocell Membranes. *Journal of the American Chemical Society* **2009**, *131* (15), 5705-5713, Article. DOI: 10.1021/ja900919c.
- (44) Evans, E.; Rawicz, W. Entropy-driven tension and bending elasticity in condensed-fluid membranes. *Phys. Rev. Lett.* **1990**, *64* (17), 2094-2097. DOI: 10.1103/PhysRevLett.64.2094.

# Supporting Information for:

---

## Ready, Set, Grow – From Micelles to Giant Vesicles via Biocatalytic Activation

*Nicholas P. Bair,<sup>a</sup> Qinyu Zhu,<sup>b</sup> Byron A. Staynings,<sup>a</sup> Douglas R. Tree<sup>b\*</sup>, Walter F. Paxton<sup>a\*</sup>*

---

<sup>a</sup> Department of Chemistry and Biochemistry, Brigham Young University, Provo, UT 84602.

<sup>b</sup> Department of Chemical Engineering, Brigham Young University, Provo, UT 84602.

*Corresponding authors
Walter F. Paxton Department of Chemistry and Biochemistry, Brigham Young University, Provo, UT 84602. Tel: 801-422-4917 E-Mail: paxton@chem.byu.edu
Douglas R. Tree Department of Chemical Engineering, Brigham Young University, Provo, UT 84602. Tel: (801) 422-5162 E-Mail: tree.doug@byu.edu

### Contents

- Figure S1. Fluorescence micrographs of MSDH suspensions at different pH.
- Figure S2. Rheology viscosity measurements at different pH
- Figure S3. Image of MSDH solutions at pH<6, pH=6, and pH>6 after 2 hours.
- Coarse-grained mapping of MSDH molecules.
- Figure S4. Coarse-grained mapping of MSDH molecules.
- Details of solvent switching protocol to obtain equilibrium structures in simulations.
- Comparison of shear rates in simulations and experiments.
- Figure S4. Velocity profile of the shear test.
- Size comparison before and after shear tests.
- Figure S6. Average diameter of MSDH aggregates before and after shear from simulations.
- Figures S7-S12. Cumulants and General Purpose fits to correlograms obtained by dynamic light scattering.

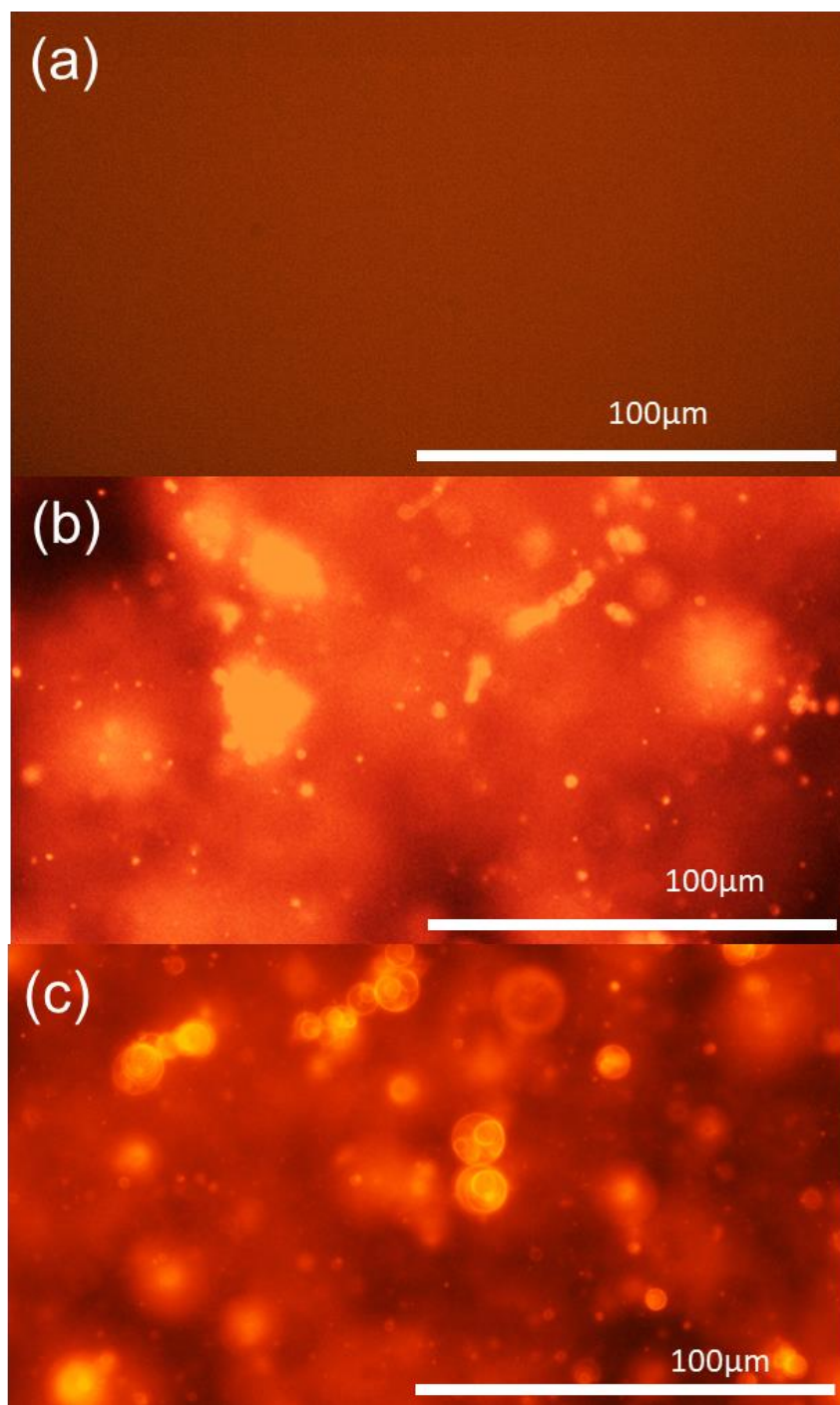


**Figure S1.** Fluorescence microscopy images of MSDH aggregates subjected to catalytic activation at (a)  $\text{pH} < 6$  showing a uniform homogeneous background; (b)  $\text{pH} = 6$  showing supramolecular aggregates  $> 10 \mu\text{m}$  near the  $\text{pK}_a$  of MSDH; (c)  $\text{pH} > 6$  showing a large number of giant vesicles. Images were acquired using a Nikon Eclipse Ti2 microscope using a  $40\times$  air objective.

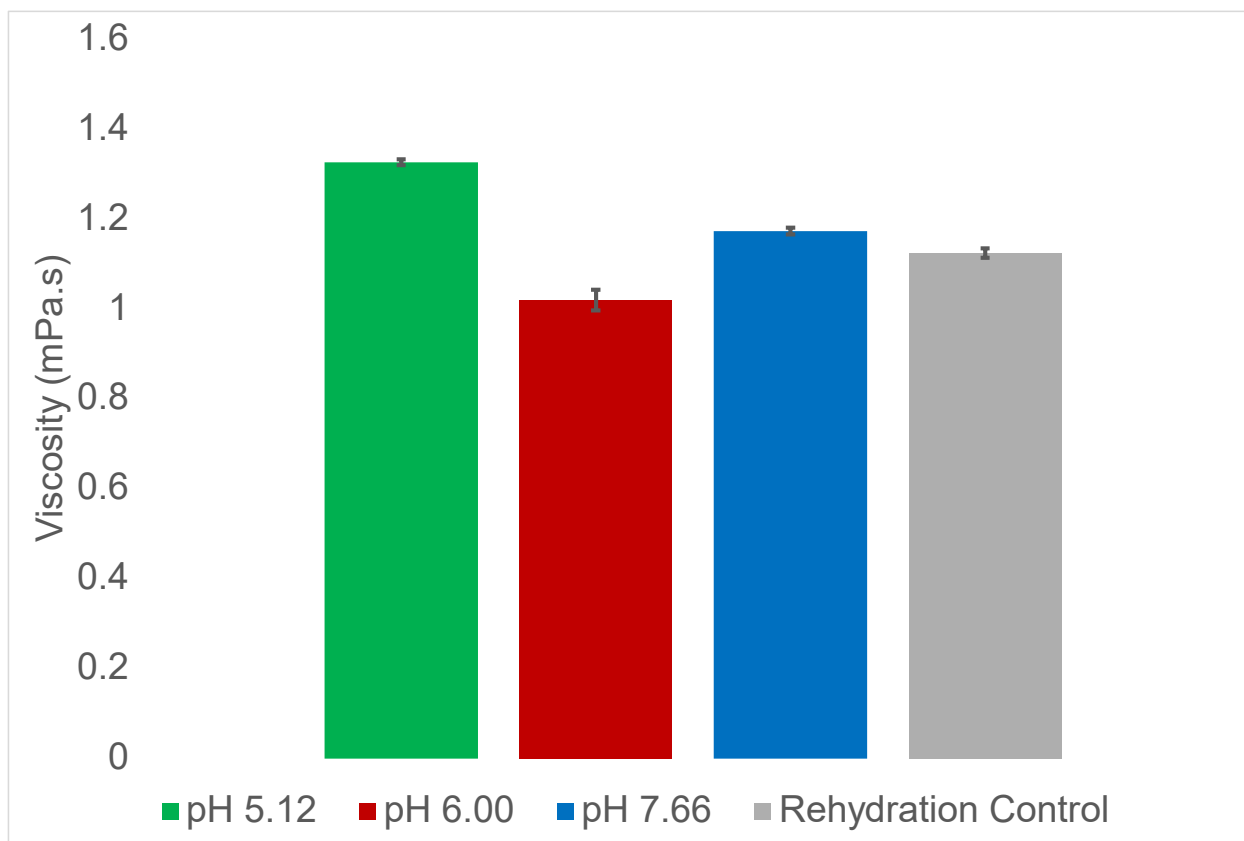


**Figure S2.** Rheological viscosity measurements at 3 different pH values and the MSDH rehydration solution control. Rheology experiments were performed with an Anton Paar MCR 302 using a PP-25 measuring device. Measurements were performed at 20 °C. Error bars are 95% confidence intervals from 30 measurements.

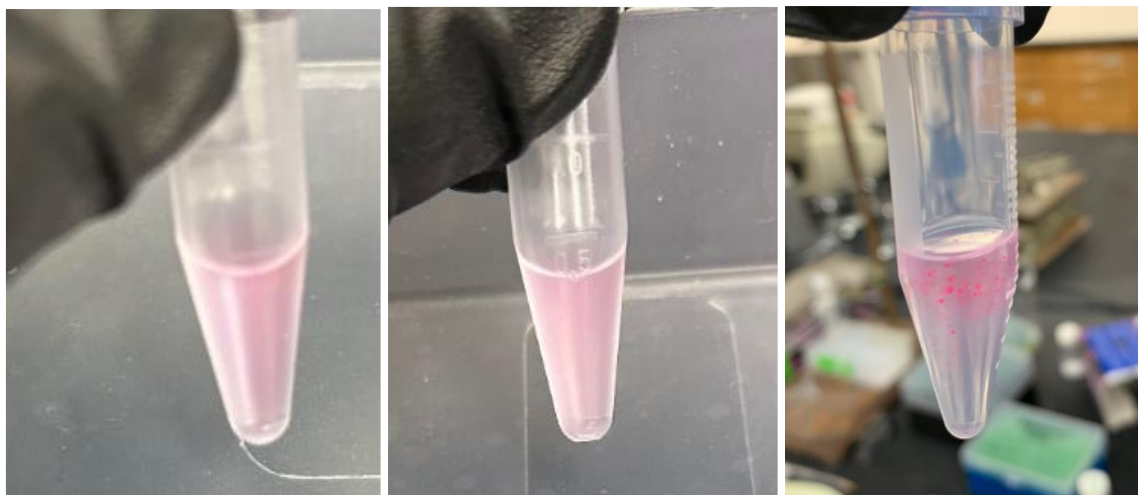


**Figure S3.** Images of MSDH with 1 mol% Texas Red DHPE at 3 pH values: pH < 6 (left); pH > 6 (center) after 2 hours; pH = 6 (right), where there were large oil like droplets suspended in the solution and the pink cloud near the droplets resulted from the tube being handled for the picture. Unintentional mixing or shaking caused some of the droplets to break apart.

**Coarse-grained mapping of MSDH molecules.** All CGMD simulations were performed using the open-source software GROMACS. We adopted the MARTINI 3 force field to model the pH responsive system, because the model is more well-developed for specific chemical species and agrees very well with experiments (*Nat. Methods* 2021, 18 (4), 382-388, manuscript reference 17). Figure S2 summarizes the coarse-grained mapping of both protonated and deprotonated MSDH molecules. We used a 3-to-1 mapping between heavy atoms and simulation beads, except for the salt species and counter ions in the protonated MSDH.

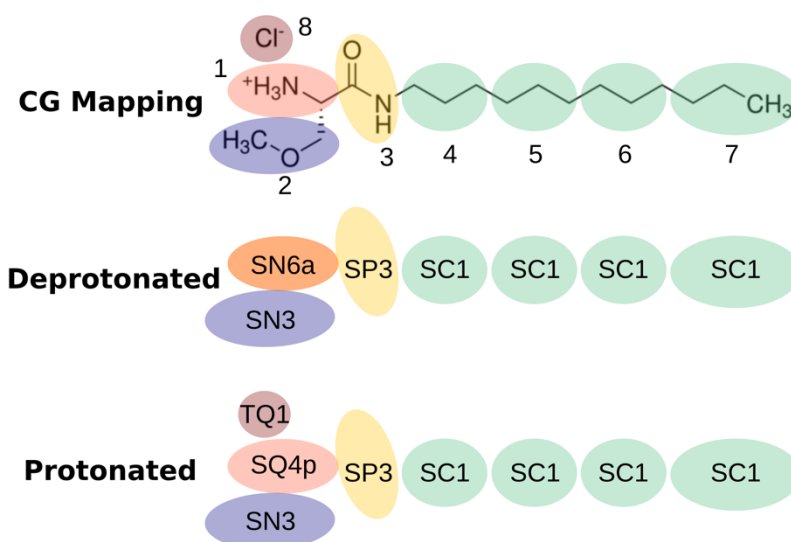


**Figure S4.** Coarse-grained mapping of MSDH molecules.

**Details of solvent switching protocol.** The equilibrium morphology diagram was constructed using CGMD simulations with explicit solvent in the NPT ensemble. In the simulations, the interaction between tail and water beads,  $\epsilon_{WT}$ , was gradually decreased, suggesting an increase in hydrophobicity, thus driving the self-assembly of MSDH surfactants. The procedure was based on a previous publication by Dong et al. (*ACS Nano* **2019**, 13, 5, 5147–5162, manuscript reference [10]). The protocol was implemented for all concentrations and protonation states, and it is meant to ensure the sampling of equilibrium structures and to avoid any kinetically trapped states.

We created a random initial configuration of 1000 MSDH molecules in a cubic simulation box, and then solvated the MSDH molecules with water to reach target concentrations. Salt concentration was maintained at 0.84 M in all cases. Temperature and pressure were set to be 300 K and 1 bar, respectively. We started out by simulating at a low hydrophobicity ( $\epsilon_{WT} = 3.22$ ) to relax the configuration away from that initial placement. We then reduced  $\epsilon_{WT}$  by 0.4 in a stepwise manner until we achieved the targeted hydrophobicity ( $\epsilon_{WT} = 0.8$ ). Each relaxation stage was simulated for 100 ns, except for the final equilibrium stage (150 ns at  $\epsilon_{WT} = 0.8$ ). We ran three replicates starting from different random initial configurations and velocities to ensure the reproducibility of the results.

**Comparison of shear rates in simulations and experiments.** We used the *cos-acceleration* tool implemented in GROMCAS to simulate the shear stress due to pipetting in manual titration case. We picked an acceleration amplitude of  $0.01 \text{ nm/ps}^2$ . We calculated the shear rate as the velocity gradient in the  $z$  direction.

$$\dot{\gamma} = \frac{\Delta v}{\Delta z}$$

The velocity profile is plotted in Figure S4. The shear rate is estimated to be around  $6.8 \times 10^{10} \text{ s}^{-1}$ , assuming a linear velocity gradient.

We also estimated the shear rate when ejecting solution from the pipette tips. We used a pipette tip of  $200 \mu\text{L}$ , with a diameter of  $500 \mu\text{m}$ . The outlet velocity is calculated as,

$$v = \frac{V}{At} = \frac{V}{\frac{\pi}{4}d^2t}$$

where  $v$  is the outlet velocity,  $V$  is the volume of the pipette tip,  $d$  is the diameter at the pipette outlet, and  $t$  is the average time per pump ( $\sim 0.25 \text{ s}$ ). The estimated velocity is  $4.074 \text{ m/s}$ . Given the velocity decreases linearly to 0 within  $1 \text{ cm}$ , then the estimated shear rate would be  $4.07 \times 10^2 \text{ s}^{-1}$ , which is a relatively high shear rate in colloidal systems. While shear rates were not quantitatively matched between simulations and experiments, the experimental shear rate was expected to disturb the growth of aggregates, or even rupture the assembled structures, which qualitatively match what we observed in simulations.

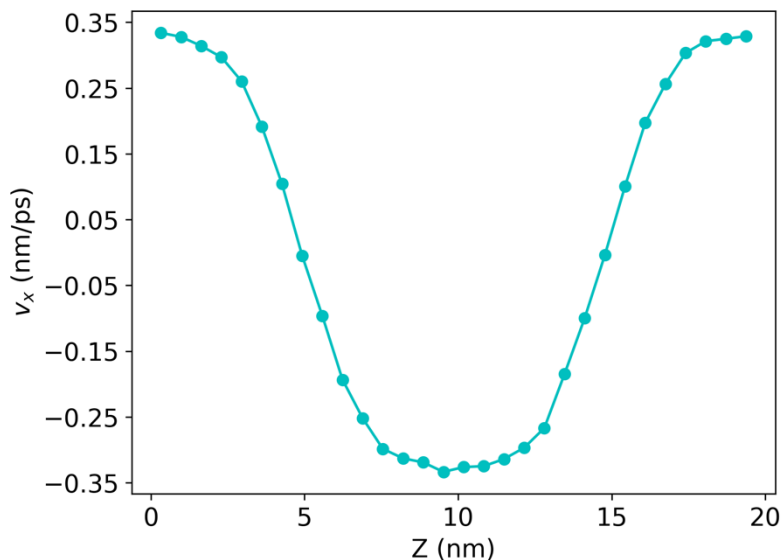


**Figure S5.** Velocity profile of the shear test.

**Size comparison before and after shear tests.** Our shear simulations of multivesicular vesicles suggested that the mechanical agitation would rupture the assembled structures, and the surfactants would only reassemble into unilamellar vesicles of smaller size. To quantify the difference, we ran three replicates using different initial conditions of multivesicular vesicles and compared the size before and after shear tests. We summarized the results in Figure S4. The average diameter of the multivesicular structures before shear is 10.40 nm (SD=0.0489 nm), with all the surfactant molecules in a single assembly. The average diameter after shear is 4.58 nm (SD=0.2834 nm). In all cases, there is a decrease in the average size after shear, suggesting that the mechanical effect would disrupt the growth of aggregates of larger size.

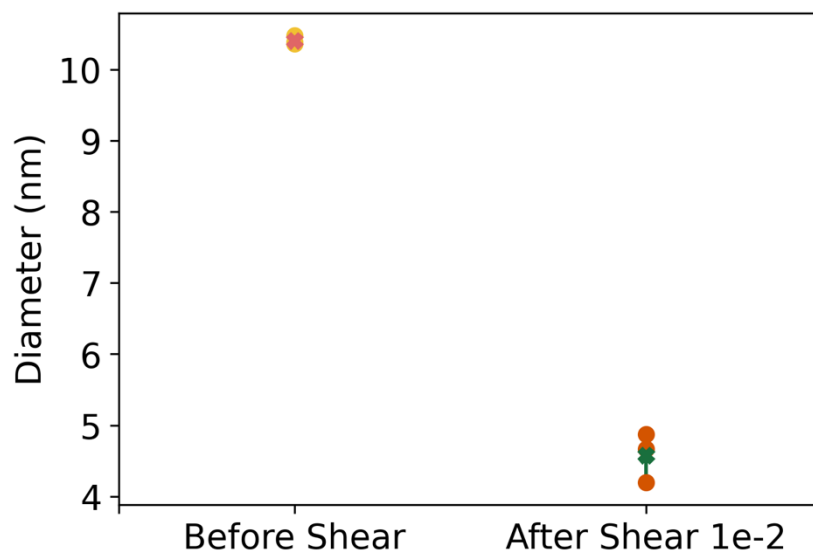


**Figure S6.** Average diameter of MSDH aggregates before and after shear from simulations.

**Figure S7.** Manual titration Cumulants fit (top) General Purpose fit (bottom) at pH<6.

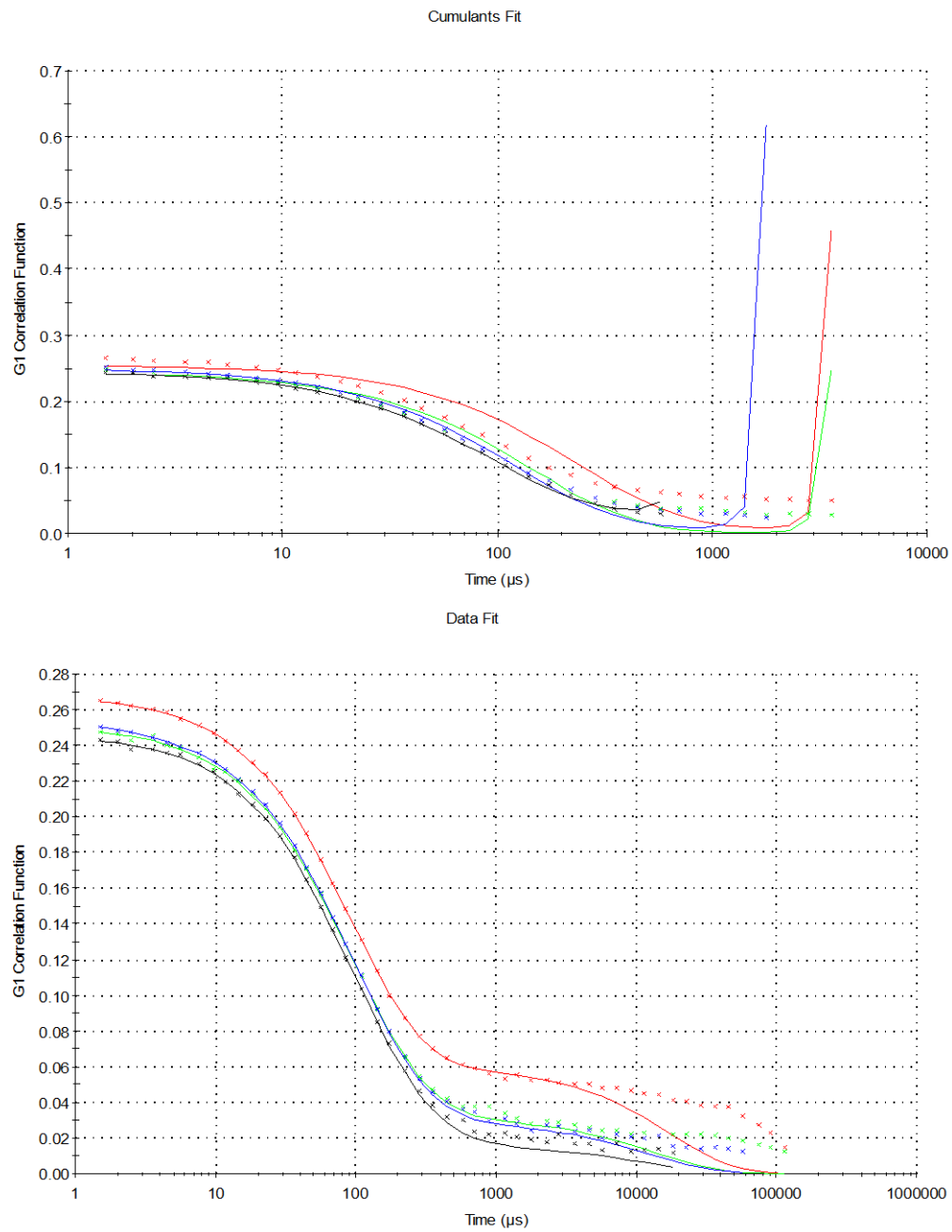


**Figure S8.** Manual titration Cumulants fit (top) General Purpose fit (bottom) at pH=6

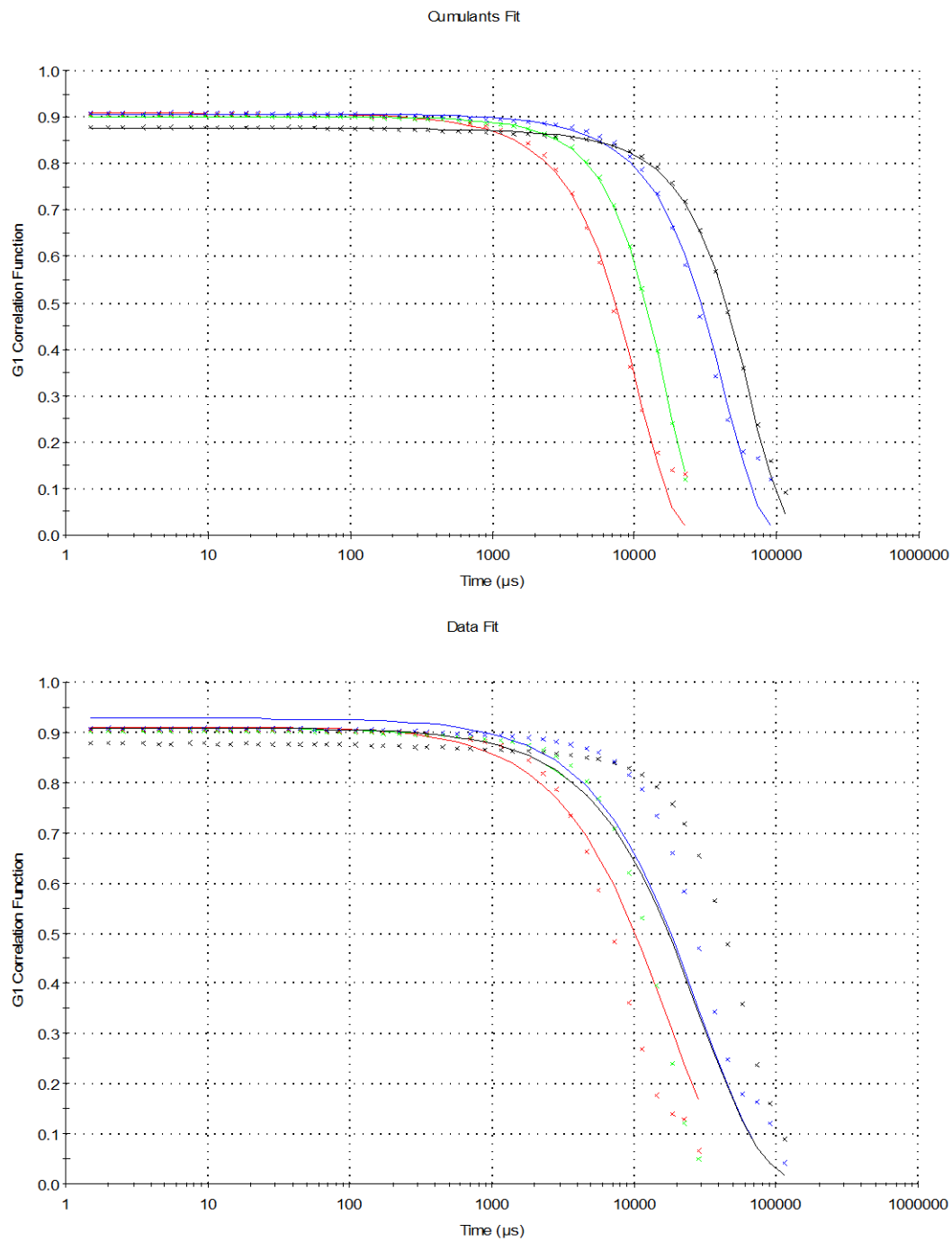


**Figure S9.** Manual titration Cumulants fit (top) General Purpose fit (bottom) at pH>6

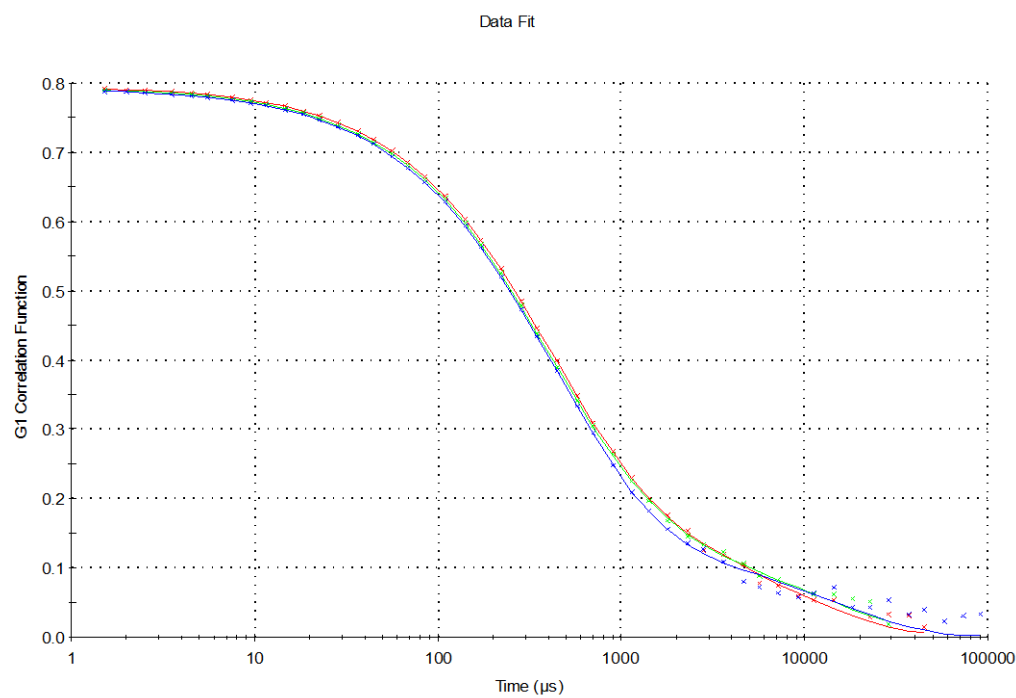
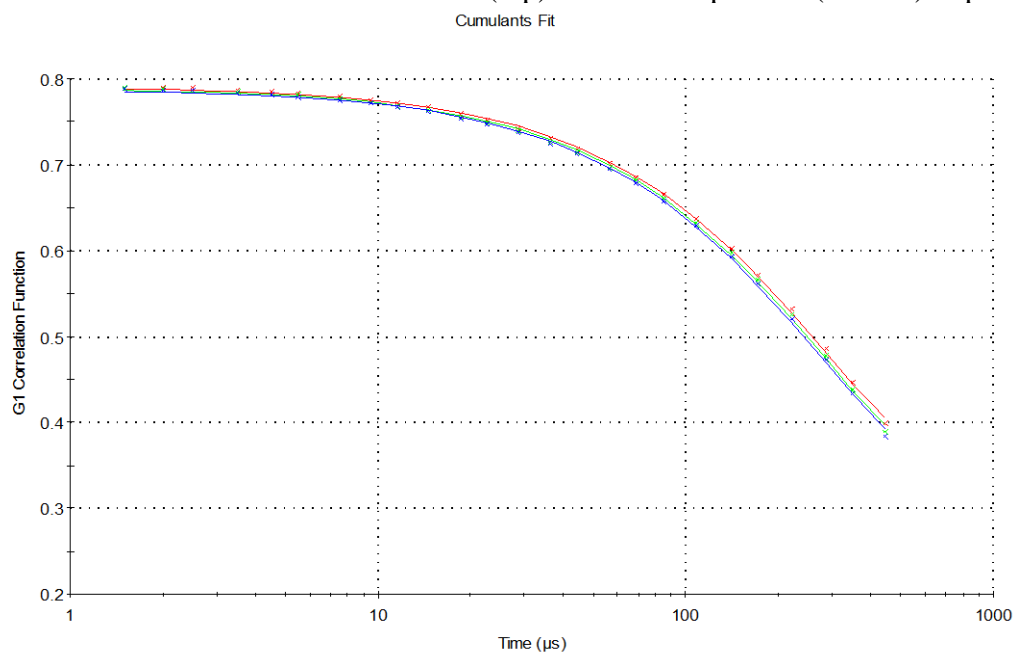


**Figure S10.** Biocatalytic (urease) titration Cumulants fit (top) General Purpose fit (bottom) at pH<6

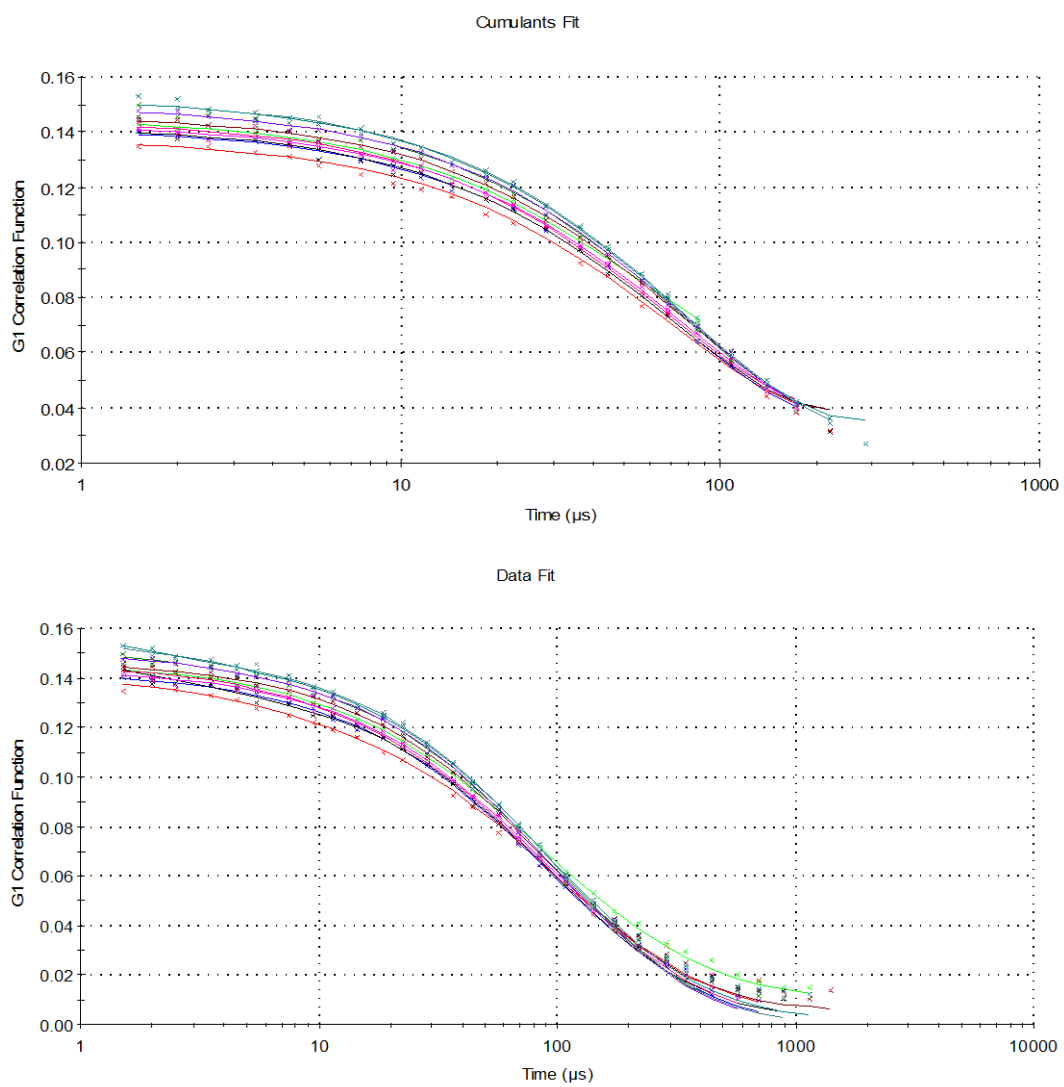


**Figure S11.** Biocatalytic (urease) titration Cumulants fit (top) General Purpose fit (bottom) at pH=6

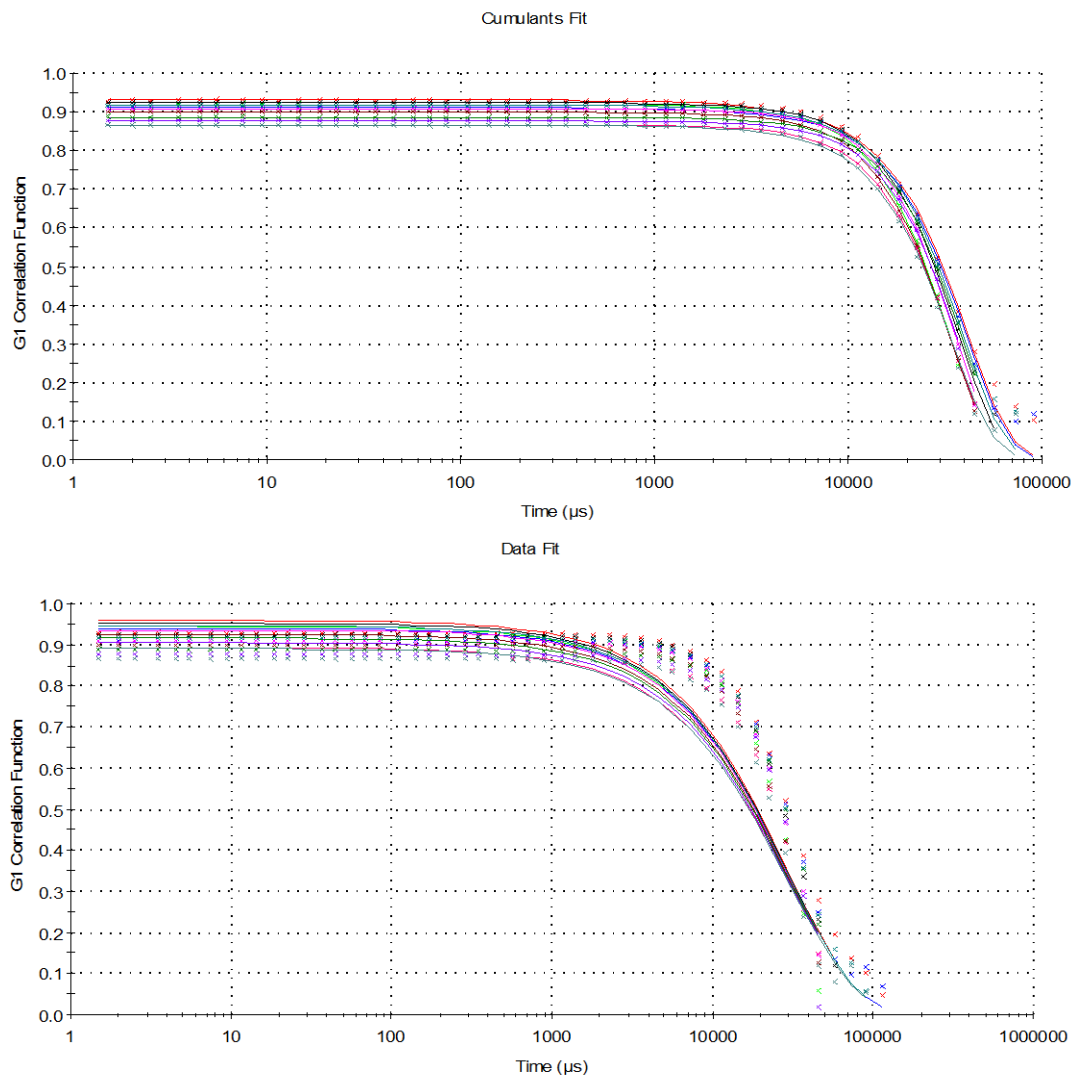


**Figure S12.** Biocatalytic (urease) titration Cumulants fit (top) General Purpose fit (bottom) at pH>6

